LAWRENCE
LIVERMORE
NATIONAL
LABORATORY

UCRL-JRNL-234346

Infrared Spectroscopy of Wild 2 Particle Hypervelocity Tracks in Stardust Aerogel: Evidence for the presence of Volatile Organics in Comet Dust

S. Bajt, S. A. Sandford, G. J. Flynn, G. Matrajt, C. J. Snead, A. J. Westphal, J. P. Bradley

September 6, 2007

Meteoritical & Planetary Science

Infrared Spectroscopy of Wild 2 Particle Hypervelocity Tracks in Stardust Aerogel: Evidence for the presence of Volatile Organics in Comet Dust

S. Bajt[1]*, S. A. Sandford[2], G. J. Flynn[3], G. Matrajt[4], C. J. Snead[5], A. J. Westphal[5], J. P. Bradley[6]

[1] Physics and Advanced Technologies, Lawrence Livermore National Laboratory, 7000 East Avenue, Livermore, CA 94550, USA,
[2] Astrophysics Branch, NASA-Ames Research Center, Moffett Field CA 94035, USA,
[3] Dept. of Physics, SUNY Plattsburgh, Plattsburgh, NY 12901, USA,
[4] Dept. of Astronomy, Univ. of Washington, Seattle, WA 98195, USA,
[5] Space Sciences Laboratory, University of California at Berkeley, Berkeley, CA 94720-7450, USA,
[6] Institute for Geophysics and Planetary Physics, Lawrence Livermore National Laboratory, 7000 East Avenue, Livermore, CA 94550, USA.

* - Author to whom correspondence should be addressed:
Saša Bajt
Lawrence Livermore National Laboratory
7000 East Avenue, L-210
Livermore, CA 94550
Phone: (925) 424 3768
Fax: (925) 423 1488
E-mail: bajt@llnl.gov

Keywords: infrared, FTIR, organics, comet, dust, synchrotron, Stardust, Wild-2, aerogel, tracks

Abstract

Infrared spectroscopy maps of some tracks, made by cometary dust from 81P/Wild 2 impacting Stardust aerogel, reveal an interesting distribution of volatile organic material. Out of six examined tracks three show presence of volatile organic components possibly injected into the aerogel during particle impacts. When particle tracks contained excess volatile organic material, they were found to be $-CH_2-$ rich. Off-normal particle tracks could indicate impacts by lower velocity particles that could have bounced off the Whipple shield, therefore carry off some contamination from it. However, this theory is not supported by data that show excess organic-rich material in normal and off-normal particle tracks. It is clear that the population of cometary particles impacting the Stardust aerogel collectors also include grains that contained little or none of this volatile organic component. This observation is consistent with the highly heterogeneous nature of the collected grains, as seen by a multitude of other analytical techniques. We propose that at least some of the volatile organic material might be of cometary origin based on

supporting data shown in this paper. However, we also acknowledge the presence of carbon (primarily as $-CH_3$) in the original aerogel, which complicates interpretation of these results.

Introduction

The Stardust mission flew through the near-nucleus coma of Comet 81P/Wild 2 on January, 2nd 2004, swept up material using aerogel collectors, and returned these samples to Earth on January, 15th 2006. Stardust is the first space mission to bring back solid material from a known body other than the Moon. After recovery of the Sample Return Capsule (SRC) the returned material was examined by the members of the Stardust Preliminary Examination Team (PET) with the goal to establish quickly and efficiently the basic nature and amount of the returned samples and disseminate preliminary observations and results. A special issue in the scientific journal Science consisting of seven papers (Brownlee et al., 2006; Flynn et al., 2006; Hörz et al., 2006; Keller et al., 2006; McKeegan et al., 2006; Sandford et al., 2006; Zolensky et al., 2006) summarized the main findings of the PET. This paper expands the data on the distribution of volatile organic components in and around the particle tracks in Stardust aerogel that was briefly reported by Sandford et al. (2006).

The captured material from the Stardust mission is unique and provides new insights into the formation of our Solar System. One of the interesting questions that the Stardust samples can address is the origin of primitive organic matter in the Solar System. To date, most of our understanding on the astrophysically-relevant chemistry of organic molecules has been obtained from telescopic astronomical observations (Pendleton et al., 1994, Sandford et al., 1991, Sandford et al., 1995, Ehrenfreund et al., 1991), from laboratory analyses of extraterrestrial materials such as meteorites and interplanetary dust particles (IDPs) (Ehrenfreund et al., 1991; Flynn et al., 2003; Flynn et al. 2004; Matrajt et al., 2005), and from laboratory simulations of the formation and evolution of organic molecules in relevant astrophysical environments (Bernstein et al., 1999; Bernstein et al., 2002; Muñoz-Caro et al., 2002). Such studies have yielded important information about the nature of extraterrestrial organics. However, remote observations are limited in the information they can provide. In addition, collected samples in the form of meteorites and IDPs are all 'orphans,' in the sense that they cannot be associated with specific parent bodies, making it somewhat difficult to put findings from them in proper context. Thanks to Stardust, we now have cometary dust from a known comet (comet 81P/Wild2), that is thought to have undergone little parent body processing (Brownlee et al., 2006; Sandford et al., 2006), and which has suffered minimal space exposure prior to collection (Brownlee et al., 2006). This material provides a unique opportunity to examine primitive Solar System organics.

Comet 81P/Wild 2 is thought to have formed in the outer region of our planetary system, after which it was ejected into the Kuiper Belt (Brownlee et al., 2006). It was selected as the target comet for the Stardust mission for several reasons. First, it is currently in a favorable orbit for relatively low velocity flybys with small spacecraft (Brownlee et al., 2003). Thus, the dust hit the aerogel with "relatively" low velocity of 6.1 km/s. Second, it has only been in its current orbit since September 1974 and has therefore made only a

modest number of passes close to the Sun. Prior to 1974, when the comet had the close encounter with Jupiter, that injected the comet into its current orbit, it was in an orbit that fell entirely outside the orbit of Jupiter. This makes Wild 2 a good candidate for the collection of early solar system materials that have undergone relatively little parent body processing.

The captured particles ejected by the comet were largely associated with two of the many jets seen to come from the nucleus (Yelle et al., 2004) and are expected to be representative of the interior of the comet rather than its surface (Brownlee et al., 2006). These particles were captured in low density aerogel at a velocity of 6.1 km/s relative to the spacecraft. Aerogel is an extremely low-density, microporous silica material that proved efficient capture of small particles at speeds of 6-7 km/s (Tsou 1995; Brownlee et al., 2003; Tsou et al., 2003; Burchell et al., 2006). The aerogel in the cometary tray had a density gradient with the lowest density near the front surface of the tiles in order to provide small particles with the gentlest possible deceleration, and increasing density with depth to provide greater stopping power for larger grains. The cometary aerogel tiles were 3 cm thick and were predicted to stop grains as large as ~ 200 μm in diameter (depending on their composition and structure). The captured particles are believed to be exposed to space for a maximum of few hours after release from the comet and therefore some volatile components, such as ices and volatile organics, could potentially have been present in the impactors, especially in larger particles (Brownlee et al., 2006). However, it is expected that due to hypervelocity impact all particles experienced some modification during the capture.

This paper reports our observations of labile organics and other volatile material distributed in aerogel along and around some particle impact tracks. The measurements were performed with synchrotron-based infrared microspectrometers with ~1000 times higher flux and ~100 times better signal/noise ratio as compared to conventional laboratory infrared spectrometers. Infrared spectroscopy is a powerful technique for direct observations of dust and ice composition in many astrophysical environments, including comets, and allows for direct comparison with extraterrestrial and standard materials analyzed in the lab. We tried to address the following questions associated with these materials: (1) Did we capture volatiles from Wild 2 cometary dust? (2) Did they change during the capture in aerogel and how? (3) What can we learn about the original chemistry of impact particles from these data?

Materials and Methods

Sample Preparation

“Keystone” samples, i.e., aerogel wedges containing whole particle tracks along with the original surface of the collector tile were prepared using a technique developed at the Space Sciences Laboratory, U. C. Berkeley (Westphal et al., 2004). The aerogel is cut by repetitive “poking” of micro-needles held by computer controlled micromanipulators attached to the stage of the extraction microscope. First, an angled cut is made which undercuts the deepest feature of a particular impact; then a vertical cut is made around the impact. The resulting wedge-shaped block of aerogel (a “keystone”) contains the entire

impact track and the terminal particles. The keystone is then removed from the collector using silicon micro-forks that are inserted into pre-machined holes in the keystone at a location to the side of the track in the tile's original surface. An example of a "keystone" with a bulbous shaped track is shown in Fig. 1. In some cases the track was sliced into multiple cross-sections. These specialized samples are prepared by laying a keystone on its side and using the same aerogel cutting tools to dissect or slice wafers of the track bulb. Such thin aerogel slices are then sandwiched between two standard transmission electron microscope Cu grids.

Methods

The results presented in this paper were obtained at two synchrotron based Fourier transform infrared (FTIR) microscopes, the National Synchrotron Light Source (NSLS) at Brookhaven National Laboratory (Upton, NY) and the Advanced Light Source (ALS) at Lawrence Berkeley National Laboratory (Berkeley, CA). These synchrotron sources, which are about two to three orders of magnitude brighter than a blackbody source, provide high brightness (power/unit area) beams and enable imaging with diffraction limited beam spots. This yields the advantage of very high sensitivity compared to conventional laboratory IR spectrometers and allows one to do molecular and compositional analysis in very small spots with high signal-to-noise ratios (Holman and Martin, 2006). Infrared spectroscopy also has the advantage that it is a very noninvasive technique that is sensitive to chemical functional groups in molecules and can therefore provide considerable information about the chemical nature of a sample without altering or destroying it.

Both systems consist of a source of infrared light (the synchrotron), an interferometer, a microscope equipped with an infrared detector, and a data recording and analysis system. The ALS beamline 1.4.3 is equipped with a ThermoNicolet Magna 760 FTIR bench and a SpectraTech Nic-Plan IR microscope. The FTIR bench used a KBr beamsplitter and the transmitted light was collected with a Mercury Cadmium Telluride (MCT-A) detector between 650 and 4000 cm^{-1} with 4 cm^{-1} spectral resolution. Spectra were normalized to the spectrum of the beam through the air and typical collection times on keystone samples were between 6 and 60 seconds per position. Aerogel keystones held with silicon microforks were attached to a specially made substrate holders that fit into the microscope slide holder and were placed directly under the microscope objective. In this way, the sample could be moved under the microscope with sub-micron precision utilizing a software stage control while the synchrotron beam remained fixed. Optical and infrared beams were aligned prior to each session and after each synchrotron beam refill, which typically occurs every 8 hours, in order to have a perfect match between optical and infrared images.

The NSLS beamline U10 is built on a bending magnet port of the VUV ring (Carr et al., 1999). The beamline delivers diffraction limited beam and is optimized for infrared microscopy/microspectroscopy. The NSLS measurements reported in this paper were made on a Nicolet Continuum FTIR microspectrometer, equipped with a fixed Ge/KBr beamsplitter, two Schwarzchild all-reflecting objectives (15X and 32X), automated X-Y scanning stage for spectroscopic mapping with 1 μm step resolution and two MCT

detectors that cover the wavenumber range from 450 to 4000 cm^{-1}. The analyses were made by obtaining an air background, then measuring the absorption of the keystone containing the particle track, using analysis spots of 10 μm x 10 μm to 20 μm x 20 μm.

Contamination Control and Assessment

After extensive laboratory experiment testing of different capturing materials it became clear that the capturing material for the Stardust comet dust return mission had to satisfy at least two conditions: (a) it had to be of sufficient low density to gradually decelerate and capture the particles and (b) it had to have high surface area to adsorb any volatiles. Silica-based aerogel was proposed to be used due to its transparency, low density, and fine mesostructure (Tsou, 1995; Tsou et al., 2003). The Stardust silica aerogel was fabricated by the two-step sol-gel process followed by high temperature supercritical point extraction and a mild vacuum-bake cycle at 300°C (Tsou, 1995; Tsou et al., 2003). The STARDUST cometary cells have several formats – some cells consists of three density layers with the lowest density (5 mg/ml) being on the top surface of the aerogel cells and the highest density (50 mg/ml) on the bottom, while others have continuous density gradients with the lowest density aerogel near the surface. The density gradient aerogel does not compromise sample survival efficiency while at the same time decreases the total thickness of the cells and increases the maximum particle size that can be captured. Due to its high surface area, aerogel is also ideal medium to adsorb any volatiles entrapped in the dust particles. However, density varies from cell to cell and batch to batch. FTIR spectroscopy was one of the techniques that measured aerogel organic contamination prior to launch (Sandford, private communication) and it was established that the initial aerogel was rich in aliphatics ($–CH_3$). It was also demonstrated that mild heating substantially reduced the residual organics. Prior to flight, all aerogel was heated to 300°C for 72 hours to reduce organic contamination. Exposure to higher temperatures would have removed a greater portion of the initial aerogel organics, but was not used because higher temperatures caused a shrinkage problem with the aerogel tiles. Nevertheless, it has been estimated that the carbon content after the heating was less than a few percent by mass (Sandford et al., 2006, 2008).

Fig. 2 shows infrared spectra of seven year old aerogel samples from three different aerogel batches (E232, E235, E236) prepared at the same time as the Stardust aerogel. These aerogels never left the Earth and were stored for the last 7 years in dry nitrogen. They provide a baseline for initial Stardust aerogel composition. We notice subtle differences among them, in particular in the strengths of the -OH and $–CH_3$ bands. All three samples show peaks due to O-Si-O bonds characteristic for aerogel, a broad peak between 1100-1200 cm^{-1} and a peak at 810 cm^{-1}. Sample E232 also displays peaks at 3742 cm^{-2}, 1649 cm^{-1}, and 975 cm^{-1}, which are attributed to –OH groups. A sample from another batch, E235, shows these same peaks, but their intensity is weaker as compared to E232. This sample has an additional peak at 2971 cm^{-1}, attributed to $–CH_3$. In the third sample, E236, we find only $–CH_3$ peak at 2971 cm^{-1} and a very weak peak associated with -OH. These measurements indicate that the aerogels made in different batches can be distinguished based on their FTIR spectra. They also confirm that some initial

contamination of –OH and $–CH_3$ is present. To distinguish between cometary organics and contamination from the spacecraft we also measured aerogel from the aerogel coupon that flew on the Stardust spacecraft but that was not exposed to the comet. In Fig. 3 we compare its infrared spectrum with one of the aforementioned aerogel samples (E236) that did not fly on the spacecraft. The FTIR spectrum of the unexposed aerogel from the Stardust spacecraft (aerogel coupon) is dominated by the O-Si-O bonds but shows also a peak at 2971 cm^{-1} ($-CH_3$) and at ~3742 cm^{-2} (-OH). Hence, from a FTIR point of view we find two types of contaminants in the original, unexposed aerogel, –OH (~3742 cm^{-1}) and $–CH_3$ (2971 cm^{-1}). Depending on the batch the aerogel tile is from, they can be present either by themselves or together. Another important observation is that the aerogel coupon shows the same contaminants as the aerogel that remained on Earth indicating no additional contamination from the spacecraft, long exposure to space or landing.

Results

Tracks C2115,22,20 and C2115,23,21 (from the same cell) were examined with the NSLS FTIR microscope. Both tracks showed a fairly typical 'ginseng' shape, and had comparable lengths of ~900 μm (Fig. 1 shows one of them, C2115,22,20). Initially, infrared spectra in these tracks were normalized to spectra taken from nearby aerogel located just outside the track. This was done in an attempt to minimize the spectral contributions of the aerogel itself. However, this effort yielded confusing results in which the residual spectral features were quite weak and varied in strength depending on which background spectrum was used to ratio the in-track spectrum. It ultimately became apparent that the problem was the background spectra being used; instead of representing true background spectra, they were themselves 'contaminated' with the sample.

This issue was dealt with by taking a series of spectra that traversed perpendicularly across both tracks at regular intervals, and normalizing each spectrum to the spectrum of air. The resulting spectra in the 3100-2750 cm^{-1} (3.23-3.64 μm) C-H stretching region are shown in Figs. 4 and 5 for the 'south' traverses from each track's center outwards. The north traverses (not shown) are very similar. Since the spectra are normalized to the air, the absorption features consist of a combination of any cometary sample present and the aerogel. The presence of cometary sample is therefore indicated by the presence of excess absorption over that seen for the aerogel alone.

It is apparent from Fig. 4 that additional non-aerogel material is indeed present in and around track C2115,22,20. However, this material is not restricted solely to the confines of the physical impact track, but instead extends outward an additional ~150-200 μm beyond the nearest edge of the track. A similar dispersion distance is seen on both sides of this track. The most obvious additions are additional absorption features near 2985 and 2935 cm^{-1}. The feature at 2935 cm^{-1} falls at a location characteristic of the asymmetric C-H stretching vibration of aliphatic $–CH_2-$ groups. The strongest aerogel band in the C-H stretching region falls near 2970 cm^{-1} and is due to asymmetric stretching associated with $–CH_3$ groups, the dominant form of contaminant carbon in the flight aerogel (Sandford et al., 2006). The feature at 2985 cm^{-1} falls at too low a frequency to be associated with C-H stretching in aromatic materials, but falls above the frequencies associated with the

normal single bonds of aliphatic materials. This feature might be explained by the presence of olefins. Olefinic bonding is seen in the C-XANES spectra of some Stardust organics as well (Sandford et al., 2006; Cody et al., 2007).

In contrast to aforementioned track the infrared spectra taken from traverses of track C2115,23,21 show no excess C-H stretching absorption beyond that of the surrounding aerogel (Fig. 5), implying that little or no additional organics are present in this track. While it is possible that there may be a cometary component of excess $–CH_3$ absorption at this spectral location, the strength of the aerogel feature precludes its unequivocal detection from these data, and the amount of material in this form must be considerably less than implied for $–CH_2-$ in the other track. This is consistent with the spectral interpretations of organics in a number of Stardust samples that indicated that the captured cometary materials show considerably higher $–CH_2-/-CH_3$ ratios that seen in the diffuse interstellar medium and in meteorites (Keller et al., 2006; Sandford et al., 2006; this paper). In this respect, the cometary samples resemble IDPs, which also show larger $–CH_2-/-CH_3$ ratios (Flynn et al., 2004; Matrajt et al., 2005).

These results made it apparent that IR spectroscopy of individual points along the impact tracks would not give a complete assessment of the total organic inventory of the impacting particles. Spectral 'maps' of entire tracks need to be collected if a more complete assessment of the organics associated with a given impacting particle is to be obtained. Fortunately, several spectral maps of tracks were obtained during PE at the ALS beamline at Lawrence Berkeley National Laboratory.

Data from spectral maps

Here we will present infrared spectral maps of four keystones that were measured in transmission mode at the ALS FTIR microspectroscope. Because of extremely low density (~5 mg/cm^3) of Stardust aerogel, the few hundred micron thick keystones are still transparent across the entire spectral region of interest (except few data points at ~1000 cm^{-1}). Each point in the map contains a full FTIR spectrum from 650 to 4000 cm^{-1} (see Methods section for more details about the experimental setup). Excess absorption at the vibration frequencies of particular bonds reveals material not present in the original aerogel. In the following we will describe in detail the data collection and processing procedures and show them step by step on one example, an IR map of particle track C2009,7,62. The optical image of the mapped area is shown in Fig. 6a. Black solid lines outline the edges of the keystone and indicate the track entrance and direction. The original aerogel surface exposed to the comet is on the left hand side.

The infrared maps (x, y, full spectrum) were collected in transmission and normalized to the air spectrum, which is basically the spectrum that the synchrotron beam sees on its way to the detector with no sample present. From these raw spectra (Fig. 6b) we calculate the optical depth of the observed absorbance features [i.e., $\tau = -\ln(I/I_o)$]. Fig. 6c shows as an example the depth of the absorbance feature at 2926 cm^{-1}, characteristic of $–CH_2-$ band and not present in the original, unexposed aerogel. The background corrected peak value

for all absorbance features of interest results in multiple maps, (x, y, value) where the value corresponds to the background corrected absorbance of a particular band. Next, we make a thickness and composition correction due to aerogel. This is done by extracting the background corrected peak values for all functional groups of interest in a point far away from the track ("clean aerogel") and then correcting each pixel in our maps for this aerogel contribution.[1] A full absorbance spectrum of a "standardized" aerogel (aerogel far away from the track) is shown in Fig. 7. In fact, several spectra of standardized aerogel are displayed to show that the spectra of "clean aerogel" within the same keystone are very similar and do not contribute more than few % error in the final calculations. The results are absorbance maps of excess materials identified by these functional groups. Fig. 8 shows such an absorbance map of the excess $–CH_2-$ material.

The absorption values, τ, from all the pixels within the map, showing excess absorption of a particular functional group, were multiplied by the relevant feature's width and divided by its intrinsic band strength as shown in Equation (1).

$$N(groups/cm^2) = \frac{\tau_i \Delta\upsilon}{A} \qquad (1)$$

where τ_i, is the depth of the absorbance feature for i-th pixel, $\Delta\upsilon$ is the spectral width of the feature and A is the intrinsic band strength for the function group. The τ_i, and $\Delta\upsilon$ values were determined experimentally from the maps (Table I) while literature values were used for intrinsic band strengths, A (Wexler, 1967; Sandford et al., 1991). Using this procedure we estimated the number of functional groups of each component present in the maps.

Four tracks (C2009,4,59; C2009,7,62; C2009,3,58; C2009,6,61) and two wafer slices (C2009,5,60; C2009,2,57) were mapped in this study. All these samples come from the same cell, C2009. As we found out later, some of the maps did not extend far enough to capture the "clean aerogel", i.e., the extended 'plumes' of organic material appear to extend out to the very edge of the cut wafers. For this reason we are not including the data from wafer slices, but will instead concentrate only on the full tracks. Three of these samples (C2009,4,59; C2009,7,62; C2009,3,58) show excess volatile components extending beyond the tracks, similar to aforementioned data from Track C2115,22,20. As an example, a change in the peak intensities in sample C2009,7,62, is plotted in Fig. 9. The intensities of the absorbance peaks ($-CH_2-$: 2926 cm^{-1}, $-CH_3$: 2963 cm^{-1}, C=O: 1720 cm^{-1}) decrease with the distance from the track, while the aerogel peak at 800 cm^{-1} remains constant. However, just as was observed in the NSLS data from track C2115,22,21, we also measured tracks with no variation in peak intensities as a function of the distance from the track (for example track C2009,6,61 in Fig. 10).

Fig. 11 shows absorbance maps from sample C2009,4,59, for $–CH_2-$, $–CH_3$, and C=O bands calculated as described above. The mapped area is about 750 x 350 μm^2. The same

[1] Because a peak due to O-Si-O vibration at ~1100 cm^{-1} (aerogel) is sometimes saturated we have used another characteristic peak near ~800 cm^{-1} for normalizing the aerogel spectral contribution.

false color bar was used for all three absorbance maps, $–CH_2$-, $-CH_3$ and C=O groups with black corresponding to 0 absorbance and white maximum absorbance. It is obvious that the $–CH_2$- band is very strong within <50 μm from the track walls and decreases rapidly with the distance from the track. It reaches the background level, present in the original aerogel, within ~100 μm from the track. The maximum absorbance of the $–CH_3$ band is about half of that observed for $–CH_2$- band but the outline of the area enriched with this compound matches that of the $–CH_2$- distribution. The third absorbance map, showing the distribution of the C=O band, is very weak as compared to $–CH_2$- absorbance map, but matches the distributions of the other spectral components in and around the track. These distribution might be related to different volatility (diffusivity) of these components, with $–CH_2$- being the least volatile and C=O and –OH (not shown) the most volatile.

In contrast, the absorbance maps obtained from sample C2009,6,61 plotted in Fig. 12 look very different. The mapped area is about 500 x 200 μm. Again, the same false color bar is used for all three absorbance maps. Only individual pixels (40 x 8 μm) show small excesses in $–CH_2$-, and possibly $–CH_3$, bands that may correlate with small organic-rich particles. They are mainly seen at the entrance of the track (left side of the images) and on the aerogel surface and could potentially also indicate contamination. The spectra, taken perpendicular to this track away from the entrance, show no changes (Fig. 10). Table I lists the number of functional groups per cm^2 (for example, N_{-CH2}) for all functional groups found in aforementioned maps.

Discussion

Infrared spectroscopy is used primarily as a qualitative, fingerprinting technique. From the baseline aerogel spectra we identified $–CH_3$ as the main organic contaminant in the original collector tiles (Figs. 2 and 3). The presence of excess absorption outside the confines of the physical impact track implies that either (i) some of the organics in the original particle were volatilized and diffused into the local aerogel during impact or (ii) that heat or shock from the impact altered carbon in the aerogel near the track.

We favor the first interpretation because data taken across similar length tracks, C2115,23,21 and C2115,22,20 show no variations in the aerogel C-H stretch spectral profile. If the spectral differences seen in the track C2115,22,20 traverse were due to impact processing of carbon indigenous to the aerogel, we would have expected to see similar processing around track C2115,23,21. This suggests that the excess organics seen in and around track C2115,22,20 represents a component indigenous to the impacting particle that made this track. Similar results were observed in C2009,7,62; C2009,4,59 (Figs. 8 and 11) and C2009,6,61 (Fig. 12) that exhibit significantly different degree and distribution of excess volatile material. This overall heterogeneity of the organic content of different grains is observed by a variety of other analytical techniques (see, for example, Sandford et al., 2006; Clemett et al., 2007; Cody et al., 2007; Matrajt et al., 2007; Rotundi et al., 2007; Spencer et al., 2007).

There is a slight correlation between track lengths and the presence of volatile components (Table II) in the tracks that were examined in this study with the shorter tracks usually showing excess in $–CH_2$-, $–CH_3$, and C=O bands while the longer ones do not. However, similar length tracks can either have excess volatiles (C2115,22,20) or not (C2115,23,21).

There are suggestions that off-normal tracks indicate particles that either bounced off or were diverted by the Whipple shield before impacting aerogel. This would lower their impact velocity and/or potentially contaminate them with Whipple shield material (Kapton). There is a lack of data in calibration rates of organics as a function of impact velocity and no data exist in the distribution of organics after the impact as taken here with FTIR microscope. Fig. 13 shows a spectrum of polyimide (Kapton) and compares it to a spectrum from a volatile rich region in Stardust aerogel. The two spectra are clearly different. In particular, strong peaks between 1600-1300 cm^{-1} in the Kapton spectrum are missing in the Stardust aerogel spectrum. Thus, the excess volatiles can not simply be explained with Kapton contamination. Additional support for this explanation is the presence of excess organics in both off-normal and normal incidence tracks and the fact that these organics are similar. This indicates the same(similar) source for these materials. If the source was only Whipple shield Kapton then the normal incidence tracks should have no excess volatile material and/or this material should be different to the off-normal incidence tracks. This is clearly not the case.

Assuming the excess volatile material is of cometary origin it would be extremely valuable to estimate the amount of carbon (organics) in the impacting particles. While this can not be done with the current data, we have attempted to calculate the number of functional groups per cm^2 from our maps. These are listed in Table I. The samples with excess volatile components (C2009,7,62; C2009,4,59) have on average about and order of magnitude higher number of functional groups per cm^2 as the samples with no excess volatiles (C2009,6,61; C2009,5,60).

Examining the ratios of $-CH_2-/-CH_3$, $-CH_2-$/C=O, $-CH_3$/C=O in organic-rich tracks (C2009,7,62 and C2009,4,59), it looks like the two tracks have very similar $-CH_2-$/C=O ratios (8.5 vs. 8.1) but considerably different $-CH_3$/C=O (3.4 vs. 8.1) and $-CH_2-/-CH_3$ ratios (2.5 vs. 1.0), i.e., $-CH_3$ is much more abundant in the C2009,4,59 track.

The $-CH_2-/-CH_3$ ratios in the samples with low excess volatile material (C2009,5,60; C2009, 6, 61) were 0.7 vs. 1.8. We estimate the ratios $-CH_2-$/C=O and $-CH_3$/C=O in the track C2009,6,61 to be 2.3 and 1.3, respectively.

Summary

Six particle tracks from two different aerogel cells (C2115 and C2009) have been examined using IR spectroscopy. Excess volatile organic material has been observed in three of them (i.e., track C2115,22,20, track C2009,4,59 and track C2009,7,62). Two of these particle tracks came from cell C2009 and one from cell C2115. When particle

tracks contained excess volatile organic material, they were found to be $–CH_2-$ rich. In addition, they contained $-CH_3$, and C=O bands. It is interesting that, independently of the original aerogel contamination (since they came from two different cells), organic-rich tracks show similar excess material. There is no correlation between the incidence angle and the presence of excess volatiles. Off-normal particle tracks could indicate impacts by lower velocity and the particle could have bounced off the Whipple shield, therefore carry off some contamination from it. However, this theory is not supported by data that show excess organic-rich material in normal and off-normal particle tracks.

All the measurements reported in this paper were made between April and June 2006, within 3 to 6 months after the Stardust landing and sample exposure to the air. Re-mapping of these tracks should show if the labile organics are stable in the air. Unfortunately most, if not all the tracks have been "used up" for other analyses.

Our analyses are only partly quantitative. In addition to present distribution of particular vibrational bands around the particle track we were able to estimate (although with large uncertainty) the numbers of functional groups per cm^2 for each track. There is still plenty of work that can be done in the future to gain more knowledge about these samples. In addition to increase the statistics by mapping more tracks from different cells there is a lack of laboratory impact studies of organic-rich material impacting Stardust quality aerogel. Most of the previous studies were performed using higher density particles, usually silicates. Also, more experimental data from impacts performed at different impact angles would be beneficial to understand the impact processes at speeds lower than 6.1 km/s. In addition, we recommend some changes for keystone preparation. Keystones need to be thin enough to be transparent but large enough so that a "clean aerogel" area can always be found beyond the outer extend of any 'plume' of collected volatile organics. Depending on the particle track size (diameter) this means an area around the track that extends over many hundreds of microns from the track walls.

Acknowledgements

We are grateful for support and samples provided by the NASA Stardust Discovery Mission and the NASA Stardust Participating Scientist Program. We thank H. N. Chapman (LLNL) for technical discussions and M. C. Martin (ALS, LBNL), Z. Hao (ALS, LBNL) and G. L. Carr (NSLS, BNL) for assistance with the experiments. Part of this work was performed under the auspices of the U.S. Department of Energy by the Lawrence Livermore National Laboratory under Contract No. W-7405-ENG-48, the Advanced Light Source, Lawrence Berkeley National Laboratory, which is supported by the Director, Office of Science, Office of Basic Energy Sciences, Materials Sciences Division, of the U.S. Department of Energy under Contract No. DE-AC03-76F00098, and the National Synchrotron Light Source, Brookhaven National Laboratory, which is supported by U. S. Department of Energy, Division of Materials Sciences and Division of Chemical Sciences, under Contract No. DE-AC02-98H10886.

References

Bernstein M., Dworkin J., Sandford S., Cooper G., and Allamandola, L. 2002. Racemic amino acids from the ultraviolet photolysis of interstellar ice analogues. *Nature* 416: 401-403.

Bernstein M. P., Sandford S. A., Allamandola L. J., Gillette J. S., Clemett S. J., and Zare R. N. 1999. UV irradiation of polycyclic aromatic hydrocarbons in ices: Production of alcohols, quinones, and ethers. *Science* 283: 1135-1138.

Brownlee D. E., Tsou P., Anderson J. D., Hanner M. S., Newburn R. L., Sekanina Z., Clark B. C., Hörz F., Zolensky M. E., Kissel J., McDonnell J. A. M., Sandford S. A., and Tuzzolino A. J. 2003. STARDUST: Comet and Interstellar Dust Sample Return Mission. *J. Geophys. Res.* 108, #E10, 8111: pp. 1-1 to 1-15.

Brownlee D., et al. 2006. Comet 81P/Wild 2 under a microscope. *Science* 314: 1711-1716.

Burchell M. J., Graham G., and Kearsley A. 2006. Cosmic dust collection in aerogel. *Ann. Rev. Earth. Planet. Sci.* 34: 385-418.

Carr, G. L., Merlo O., Munsli M., Springer S., and Ho S. C. 1999. Characterization of the new NSLS infrared microspectroscopy beamline U10B. *SPIE Proc.* 3775 in "Accelerator-based sources of infrared and spectroscopic applications", pp 22-29.

Clemett S. J, et al. 2008. Complex Aromatic Hydrocarbons in STARDUST Samples Collected from the Comet 81P/Wild-2. *MAPS*, in preparation.

Cody G. D., Ade H., Alexander C. M. O'D., Araki T., Butterworth A., Fleckenstein H., Flynn G., Gilles M. K., Jacobsen C., Kilcoyne A. L. D., Messenger K., Sandford S. A., Tyliszczak T., Westphal A. J., Wirick S., and Yabuta H. 2007. Quantitative Organic and Light Element Analysis of Comet 81P/Wild 2 Particles using C-, N-, and O- μ-XANES. *MAPS*, submitted.

Ehrenfreund P., Robert F., D'Hendencourt L., Behar F. 1991. Comparison of interstellar and meteoritic organic-matter at 3.4 μm. *A&A* 252: 712-717.

Flynn G. J. et al. 2006. Elemental composition of Comet 81P/Wild 2 Samples Collected by Stardust. *Science* 314: 1731-1735.

Flynn G. J., Keller L. P., Feser M., Wirick S., and Jacobsen C. 2003. The origin of organic matter in the solar system: Evidence from the interplanetary dust particles. *Geochim. Cosmochim. Acta* 67: 4791-4806.

Flynn G. J., Keller L. P., Jacobsen C., Wirick S. 2004. An assessment of the amount and types of organic matter contributed to the Earth by interplanetary dust. *Space life sciences: Steps toward origin(s) of life* 33: 57-66.

Holman H. -Y., and Martin M. C. 2006. Synchrotron radiation infrared spectromicroscopy: A non-invasive chemical probe for monitoring biogeochemical processes. *Advances in Agronomy* 90: 79-127.

Hörz F., et al. 2006. Impact Features on Stardust: Implications for Comet 81P/Wild 2 Dust. *Science* **314**: 1716-1719

Keller L. P. et al. 2006. Infrared Spectroscopy of Comet 81P/Wild 2 Samples Returned by Stardust. *Science* 314: 1728-1731.

Matrajt G., Muñoz Caro G. M., Dartois E., D'Hendecourt L., Deboffle D., and Borg J. 2005. FTIR analysis of the organics in IDPs: Comparison with the IR spectra of the diffuse interstellar medium. *A&A* 433: 979-995.

McKeegan K. D., et al. 2006. Isotopic Compositions of Cometary Matter Returned by Stardust. *Science* 314: 1724-1728.

Muñoz-Caro, G.M., Meierhenrich, U., Schutte, W., Barbier. B., Arcones Segovia, A., Rosenbauer, H., Thiemann, W., Brack, A., and Greenberg, J. 2002. Amino acids from ultraviolet irradiation of interstellar ice analogues. *Nature* 416:403-406.

Pendelton Y.J., Sandford S.A., Allamandola L.J., et al. 1994. Near-infrared absorption-spectroscopy of interstellar hydrocarbon grains. *ApJ.* 437: 683-696.

Rotundi, A., Baratta, G. A., Borg, J., Brucato, J. R., Busemann, H., Colangeli, L., d'Hendecourt, L., Djouadi, Z., Ferrini, G., Franchi, I. A., Fries, M., Grossemy, F., Keller, L. P., Mennella, V., Nakamura, K., Nittler, L. R., Palumbo, M. E., Sandford, S. A., Steele, A., & Wopenka, B. 2007. Combined Micro-IR and Micro-Raman Analyses of Comet 81P/Wild 2 Particles Collected by Stardust. *MAPS*, submitted.

Sandford S. A., Allamandola L. J., Tielens A. G. G. M., Sellgren K., Tapia M., Pendelton Y. 1991. The interstellar C-H stretching band near 3.4 microns: Constraints on the composition of organic material in the diffuse interstellar medium. *ApJ* 371: 607-620.

Sandford S.A., Pendelton Y.J., Allamandola L.J. 1995. The galactic distribution of aliphatic-hydrocarbons in the diffuse interstellar-medium. *ApJ* 440: 697-705.

Sandford S. A., et al. 2006. Organics Captured from Comet 81P/Wild 2 by the Stardust Spacecraft. *Science* 314: 1720-1724.

Sandford S. A., et al. 2008. Assessment and Control of Organic Contaminants Associated with the Stardust Sample Return from Comet 81P/Wild 2. *MAPS*, in preparation.

Spencer M. K., Clemett S. J., Sandford S. A., McKay D. S., and Zare R. N. 2008. Organic Compound Detection along Hypervelocity Particle Impact Tracks in Stardust Aerogel. *MAPS*, submitted.

Tsou P. 1995. Silica aerogel captures cosmic dust intact. *J. of Non-cryst. Solids* 186: 415-427.

Tsou P., Brownlee D. E., Sandford S. A., Hörz F., and Zolensky M. E. 2003. Wild 2 and interstellar sample collection and Earth return. *J. Geophys. Res.* 108:2 8113, pp. 3-1 to 3-21.

Westphal A. J., Snead C., Butterworth A., Graham G. A., Bradley J. P., Bajt S., Grant P., Bench G., Brennan S., Pianetta P. 2004. Aerogel keystones: Extraction of complete hypervelocity impact events from aerogel collectors. *MAPS* 39: 1375-1386.

Wexler A. S. 1967. Integrated intensities of absorption bands in infrared spectroscopy. *Applied Spectroscopy Rev.* 1: 29-98.

Yelle R. V., Soderblom L. A., Jokipii R. J. 2004. Formation of jets in Comet 19P/Borrelly by subsurface geysers. *Icarus* 167: 30-36.

Zolensky M. E., et al. 2006. Mineralogy and Petrology of Comet 81P/Wild 2 Nucleus Samples. *Science* 314: 1735-1739.

Tables

	C2009,7,62	C2009,4,59	C2009,6,61	C2005,5,60
$\Delta\nu_{\text{-CH2-}}$	20	20	18	20
$\Delta\nu_{\text{-CH3}}$	20	20	22	24
$\Delta\nu_{\text{C=O}}$	28	32	30	n.d.
$A_{\text{-CH2-}}$*	$8\text{x}10^{-18}$	$8\text{x}10^{-18}$	$8\text{x}10^{-18}$	$8\text{x}10^{-18}$
$A_{\text{-CH3}}$*	$1.2\text{x}10^{-17}$	$1.2\text{x}10^{-17}$	$1.2\text{x}10^{-17}$	$1.2\text{x}10^{-17}$
$A_{\text{C=O}}$*	$1.7\text{x}10^{-17}$	$1.7\text{x}10^{-17}$	$1.7\text{x}10^{-17}$	$1.7\text{x}10^{-17}$
$N_{\text{-CH2-}}$**	$1.2\text{x}10^{13}$	$4.9\text{x}10^{13}$	$1.7\text{x}10^{12}$	$6.2\text{x}10^{12}$
$N_{\text{-CH3}}$**	$4.8\text{x}10^{12}$	$4.9\text{x}10^{13}$	$9.3\text{x}10^{11}$	$8.8\text{x}10^{12}$
$N_{\text{C=O}}$**	$1.4\text{x}10^{12}$	$6.0\text{x}10^{12}$	$3.9\text{x}10^{11}$	n.d.

Table I: * The intrinsic band strengths values, A, are given in cm per functional group. ** N is the number of functional groups per cm^2. The error bars on N numbers for C2009,7,62 and C2009,4,59 are 10% and for C2009,6,61 and C2009,5,60 are about 50%.

Sample name	Approx. track length (μm)	Angle of incidence	Excess volatile component
C2009,3,58	256	Off-normal	Yes
C2009,4,59	320	Off-normal	Yes
C2009,7,62	500	Ambiguous	Yes
C2115,22,20	900	Normal?	Yes
C2115,23,21	900	Normal	No
C2009,6,61	1480	Off-normal	No

Table II: List of all examined tracks. Comparison based on their lengths, angle of incidence and presence of volatile components.

Figure Captions

Fig. 1. Track C2115,22,20. The original aerogel surface exposed to the comet is shown on the right hand side. The linescans described in Fig. 4 were done perpendicular to the track, e.g. parallel to the original aerogel surface.

Fig. 2. Infrared spectra of three flight spare aerogel tile batches, E232, E235, and E236 all showing a strong peak centered at 1125 cm^{-1} (O-Si-O), peak at 810 cm^{-1} (O-Si-O), a small shoulder peak at 975 cm^{-1} (Si-OH), and some showing 2970 cm^{-1} (-CH_3) and 3740 cm^{-1} (-OH in water or Si-OH stretch). All the spectra are plotted on the same scale (0 to 100% transmission) but are off-set for better visibility.

Fig. 3. Infrared spectrum of a portion of the aerogel 'witness coupon' that flew on Stardust but was not exposed directly to the comet. For comparison we also plot the infrared spectrum of an aerogel flight spare tile from batch E236 that was prepared together with Stardust aerogel 7 years ago, stored in dry nitrogen but never flew on the spacecraft. All the spectra are plotted on the same scale (0 to 100% transmission) but are off-set for better visibility.

Fig. 4. Details of infrared spectra taken from track C2115,22,20. The spectra were taken every 80 μm starting from the track center and are displayed off-set for better visibility.

Fig. 5. Details of infrared spectra taken from track C2115,23,21. These spectra were also taken every 80 μm starting from the track center and are displayed off-set for better visibility.

Fig. 6. (a) Optical image showing the edges of the keystone and the position of the track. The bars represent 100 μm. The mapped area is approximately 650 x 450 μm^2. (b) A snapshot of the raw transmission data (x, y, full spectrum) for the wavenumber position of 2930 cm^{-1}. (c) Absorbance data for the same wavenumber position. (d) Background corrected absorbance map for 2930 cm^{-1} wavenumber.

Fig. 7. Three different spectra showing variation in the aerogel spectra in the "clean area", far away from the particle track.

Fig. 8. Aerogel corrected map from Fig. 6 (C2009,7,62). The black color corresponds to no excess material, while white shows the highest concentration of $–CH_2-$ excess material.

Fig. 9. Details of infrared spectra taken from track C2009,7,62. All three spectra are plotted on the same scale (0 to 100% transmission) but are off-set for better visibility.

Fig. 10. Data taken from Track C2009,6,61 show no change in infrared spectra as a function of the distance from the track. All the spectra are plotted on the same scale (0 to 100% transmission) but are off-set for better visibility.

Fig. 11. Absorbance maps for $-CH_2-$ (a), $-CH_3$ (b), and C=O (c) can be compared to the optical image (d) showing the edges of the keystone in sample C2009,4,59. For easier interpretation the same false color bar is used in all three absorbance images with the black corresponding to 0 and the white corresponding to the maximum. The original aerogel surface exposed to the comet is on the left hand side. The mapped area is approximately 750 x 350 μm^2. Magnification is the same in all four images and the white bar corresponds to 100 μm. The two vertical black lines in the optical image (d) are stitches of two images.

Fig. 12. Absorbance maps of $-CH_2-$ (a), $-CH_3$ (b) and C=O (c) in track C2009,6,61. Same false color bar is used in all three images with the black (min) corresponding to 0 and the white corresponding to the maximum. The optical image (d) of the track with the same magnification as the absorbance maps is displayed in bottom right corner. The aerogel surface exposed to the comet is on the left. The mapped area is approximately 500 x 200 μm^2. Magnification is the same in all four images and the white bar corresponds to 100 μm

Fig. 13. Polyimide-Kapton (dash) vs. volatile rich Stardust aerogel (solid) spectrum. Note absence of some strong peaks between 1300-1600 cm^{-1} in Stardust aerogel. The polyimide spectrum is taken from Omnic library (Omnic is a registered trademark of Thermo Electron Corporation).

Figures

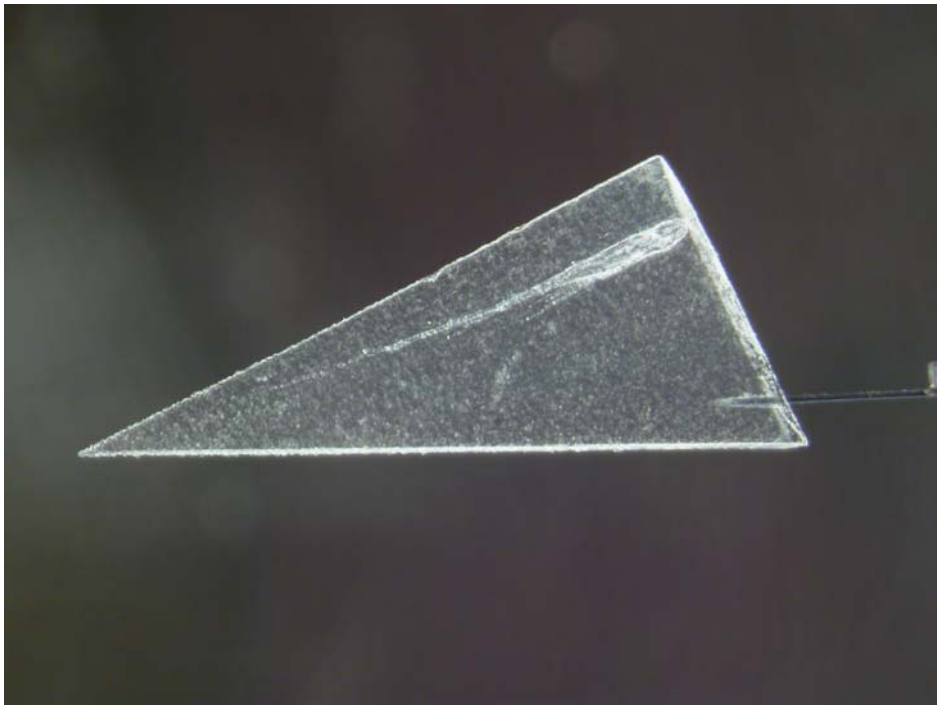

Fig. 1.

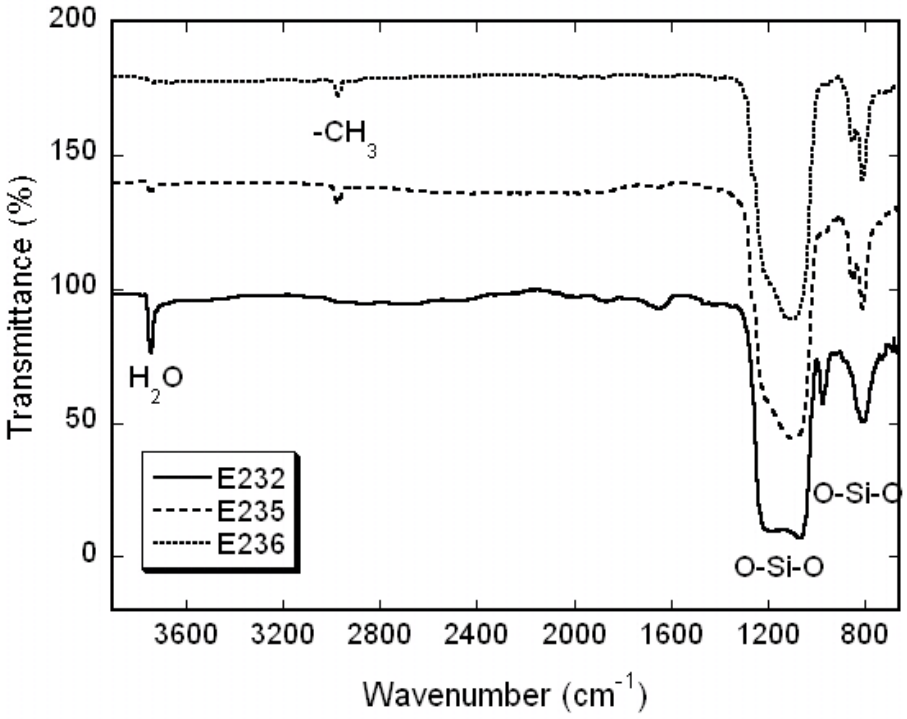
200
150
100
50
0
Transmittance (%)
-CH3
H2O
E232
E235
E236
O-Si-O
O-Si-O
3600
3200
2800
2400
2000
1600
1200
800
Wavenumber (cm-1)

Fig. 2.

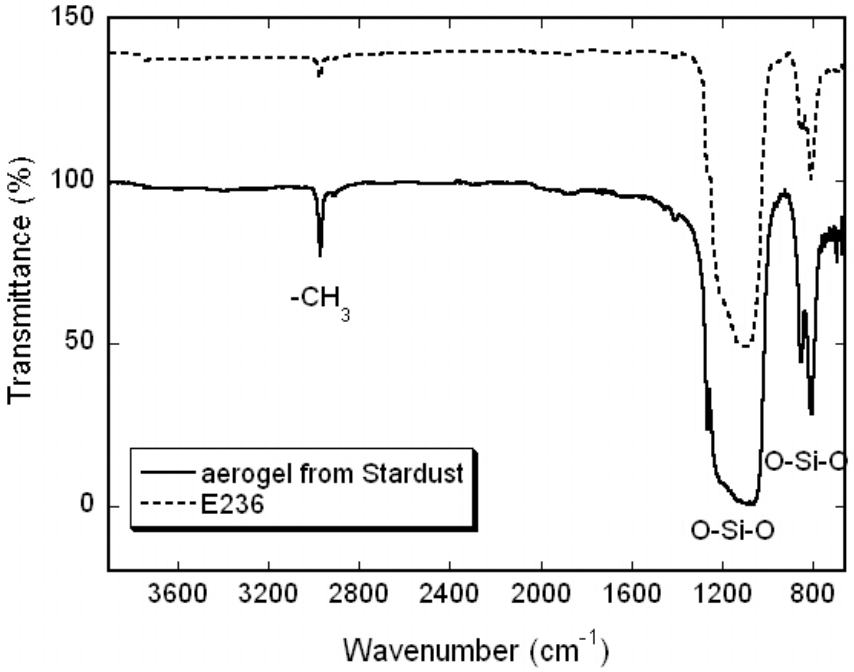
150
100
50
0
Transmittance (%)
-CH3
O-Si-O
O-Si-O
aerogel from Stardust
E236
3600
3200
2800
2400
2000
1600
1200
800
Wavenumber (cm-1)

Fig. 3.

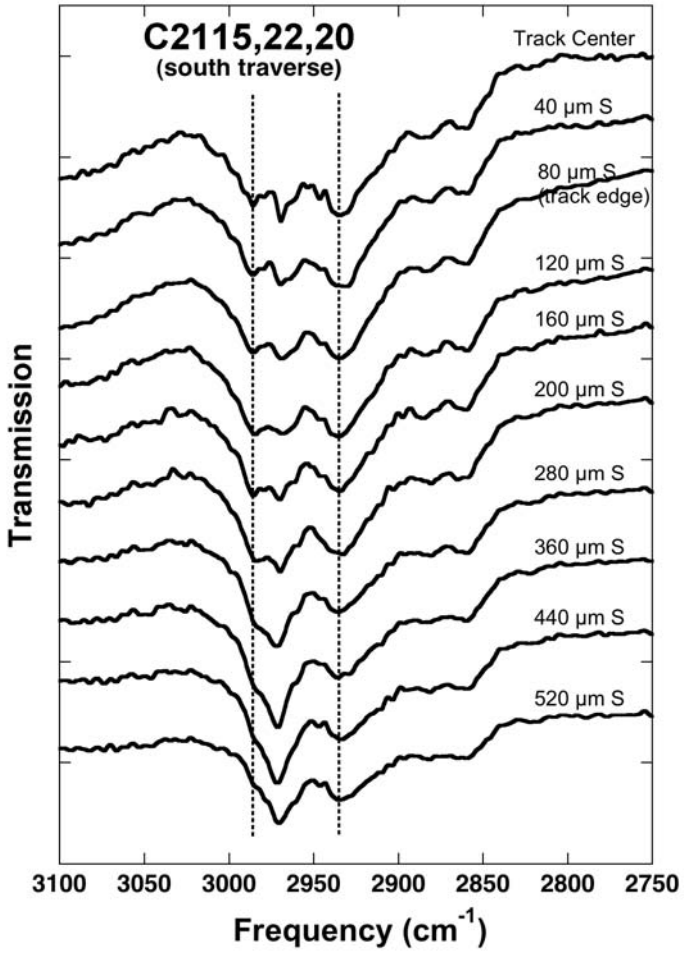
C2115,22,20
(south traverse)
Track Center
40 μm S
80 μm S
(track edge)
120 μm S
160 μm S
200 μm S
280 μm S
360 μm S
440 μm S
520 μm S
Transmission
3100
3050
3000
2950
2900
2850
2800
2750
Frequency (cm-1)

Fig. 4.

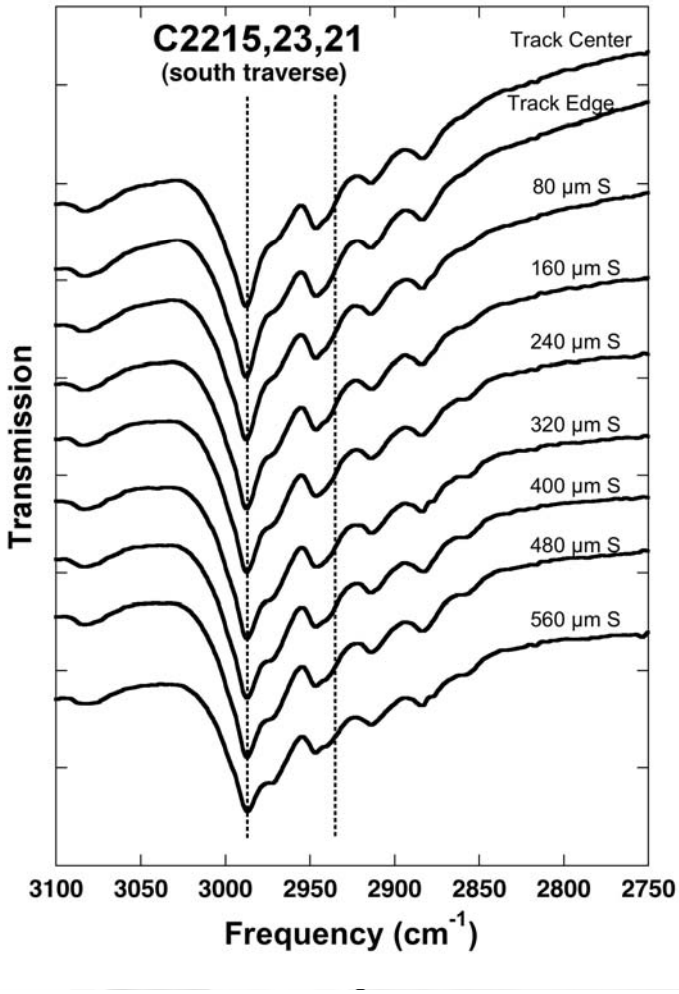
C2215,23,21
(south traverse)
Track Center
Track Edge
80 μm S
160 μm S
240 μm S
320 μm S
400 μm S
480 μm S
560 μm S
Transmission
3100
3050
3000
2950
2900
2850
2800
2750
Frequency (cm-1)

Fig. 5.

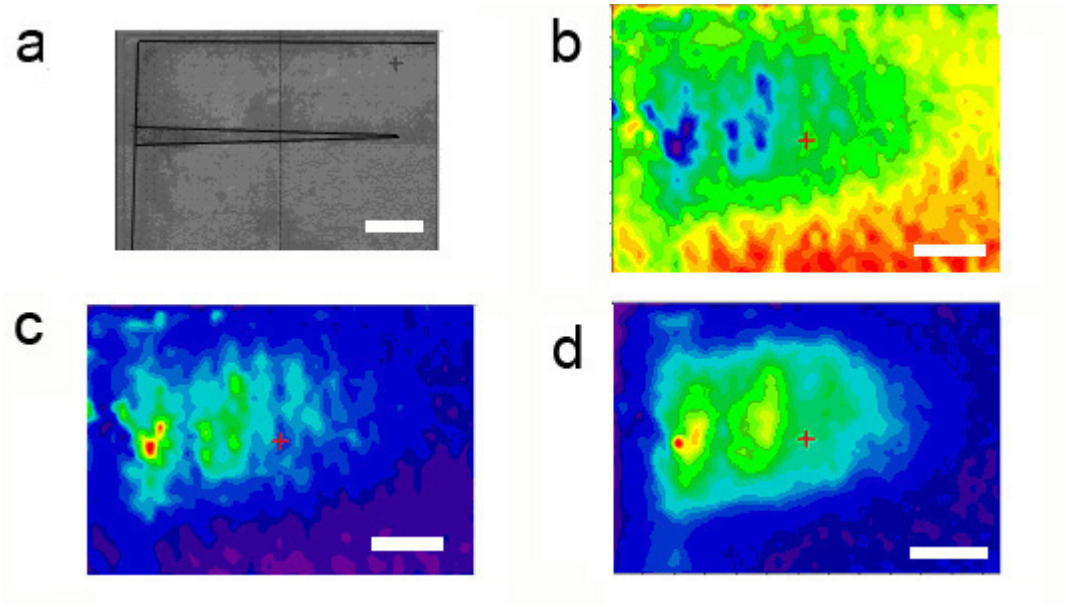

Fig. 6.

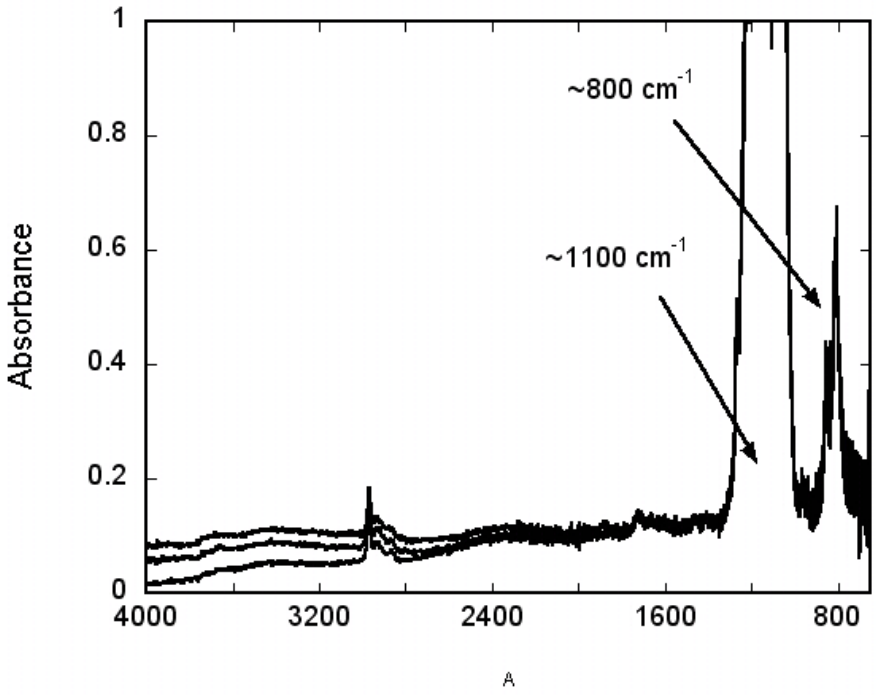
Absorbance
1
0.8
0.6
0.4
0.2
0
4000
3200
2400
1600
800
~800 cm-1
~1100 cm-1
A

Fig. 7.

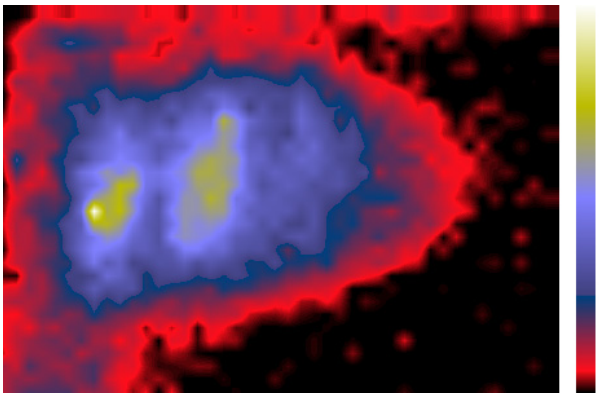

Fig. 8.

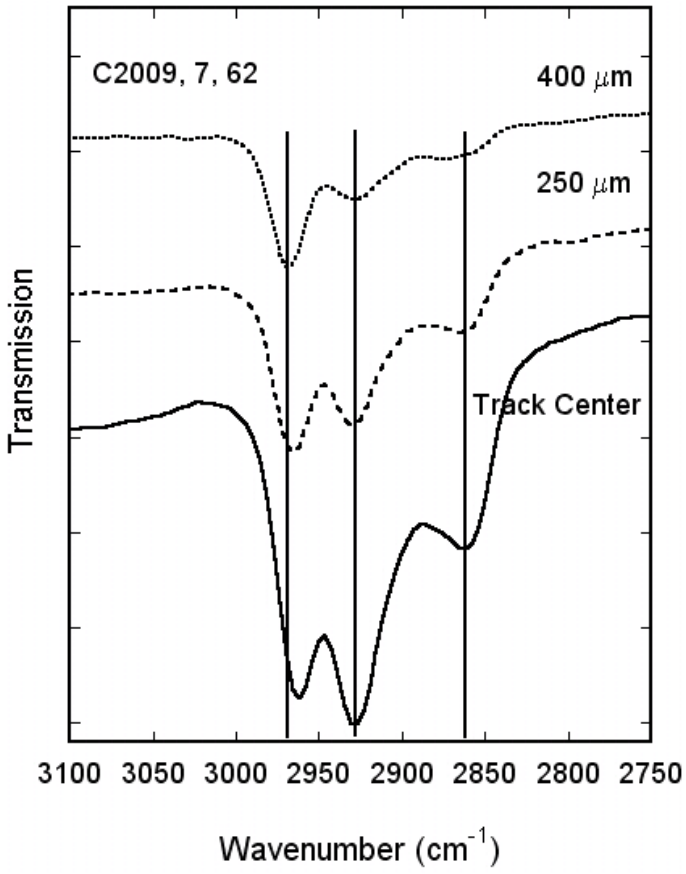
C2009, 7, 62
400 μm
250 μm
Track Center
Transmission
3100 3050 3000 2950 2900 2850 2800 2750
Wavenumber (cm-1)

Fig. 9.

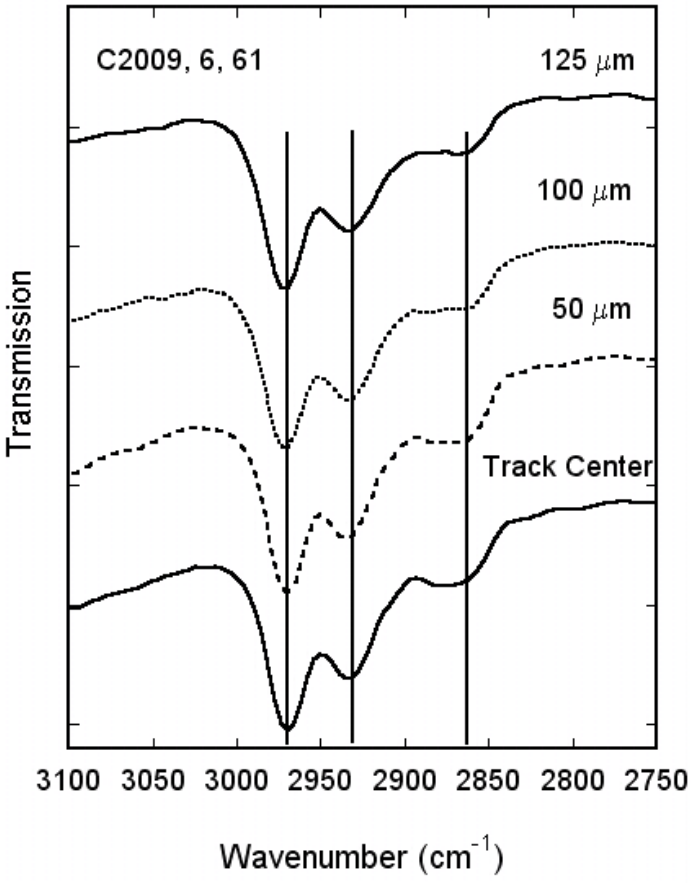
C2009, 6, 61
125 μm
100 μm
50 μm
Track Center
Transmission
3100 3050 3000 2950 2900 2850 2800 2750
Wavenumber (cm-1)

Fig. 10.

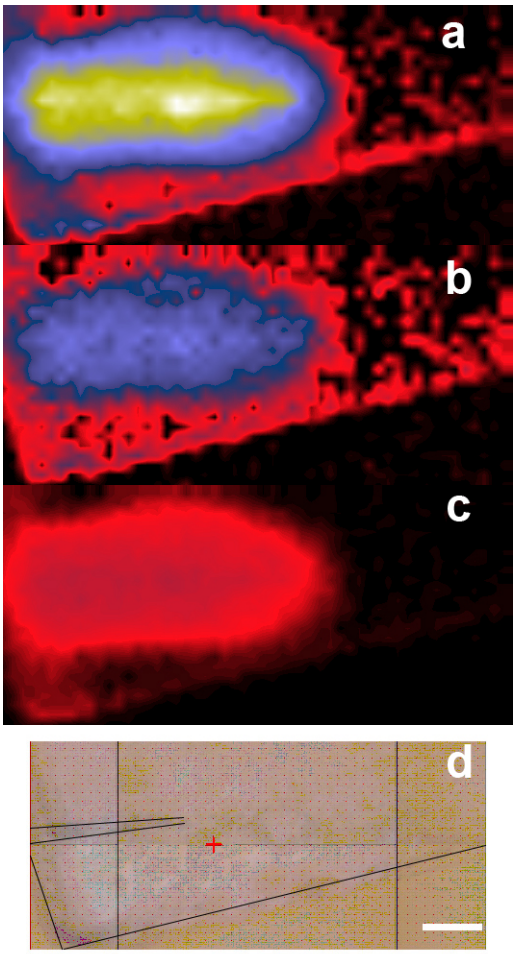

Fig. 11.

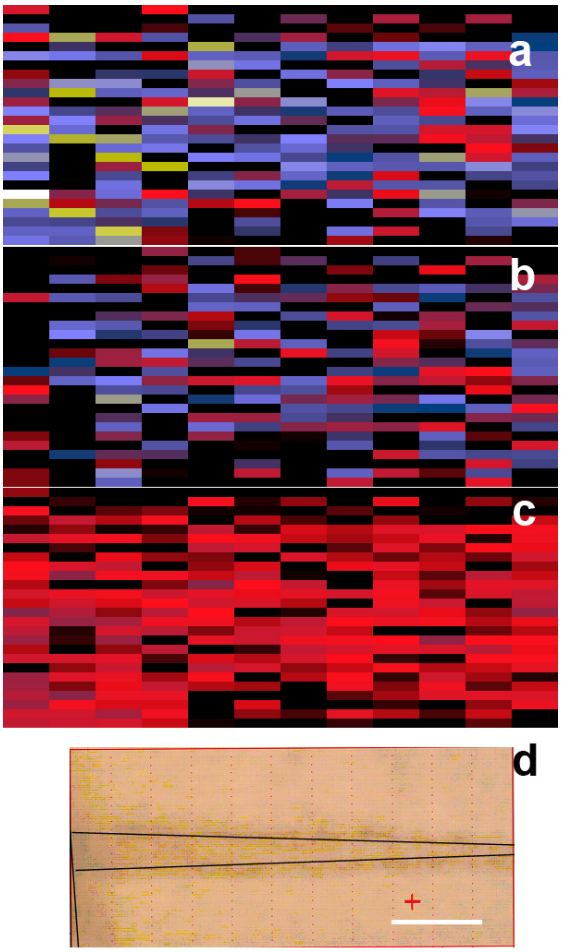

Fig. 12.

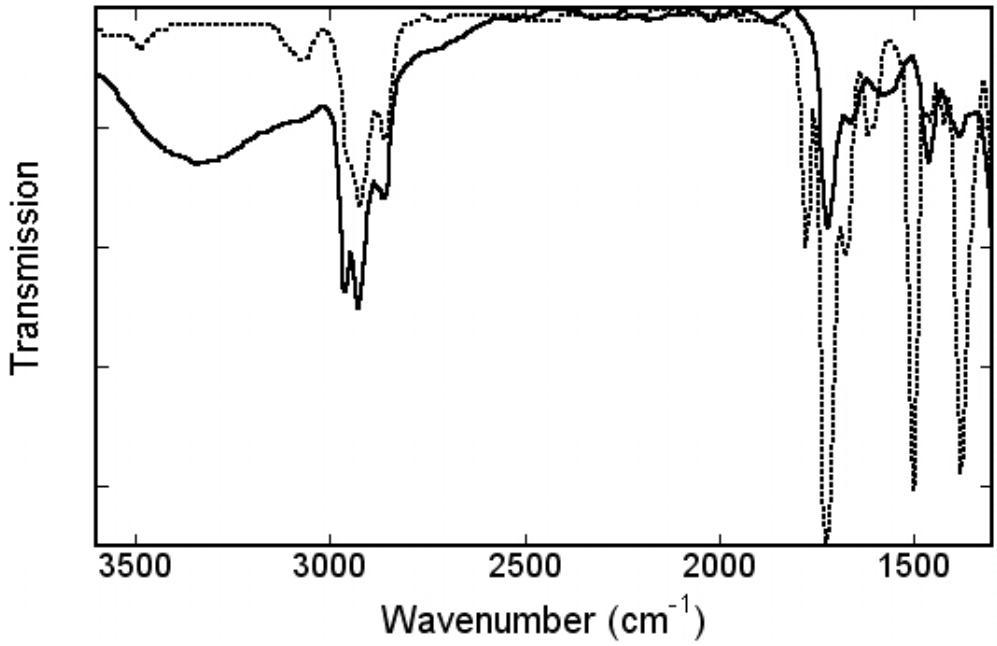

Fig. 13.